Macromolecules

Article

pubs.acs.org/Macromolecules

Structure and Dynamics of Hyperbranched Polymer/Layered Silicate Nanocomposites

S. Fotiadou,[†,‡] C. Karageorgaki,[†,‡,∥] K. Chrissopoulou,[†,*] K. Karatasos,[‡] I. Tanis,[‡] D. Tragoudaras,[‡] B. Frick,[§] and S. H. Anastasiadis[†,⊥]

[†]Institute of Electronic Structure and Laser, Foundation for Research and Technology—Hellas, P.O. Box 1527, 711 10 Heraklion, Crete, Greece

[‡]Department of Chemical Engineering, Aristotle University of Thessaloniki, 541 24 Thessaloniki, Greece

[§]Institut Laue Langevin (ILL), 6 rue Jules Horowitz, F38042 Grenoble, France

[⊥]Department of Chemistry, University of Crete, P.O. Box 2208, 710 03 Heraklion Crete, Greece

ABSTRACT: The structure and dynamics of a hyperbranched polyesteramide (Hybrane S 1200) polymer and its nanocomposites with natural montmorillonite (Na^+−MMT) are investigated to offer a detailed picture of its behavior in bulk and under confinement. In bulk, the behavior is probed by quasi-elastic neutron scattering (QENS) with molecular dynamics simulations employed for a better insight into the relevant relaxation processes. The energy-resolved elastically scattered intensity from the polymer exhibits two distinct relaxation steps, one attributed to sub-T_g motions and one observed at temperatures above the glass transition, T_g. The QENS spectra measured over the complete temperature range are consistent with the elastic measurements and can be correlated to the results emerging from the detailed description afforded by the atomistic simulations, which cover a broad time range and predict the existence of three relaxation processes. The nanocomposites are investigated by X-ray diffraction (XRD), differential scanning calorimetry (DSC) and QENS. XRD reveals an intercalated nanocomposite structure with the polymer chains residing within the galleries of the Na^+−MMT. The polymer chains confined within the galleries show similarities in the behavior with that of the polymer in the bulk for temperatures below the bulk polymer T_g, whereas they exhibit frozen dynamics under confinement at temperatures higher than that.

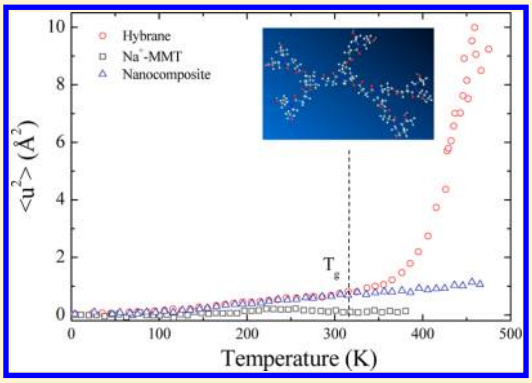

I. INTRODUCTION

The investigation of the dynamics of polymeric systems has attracted the scientific interest because of the complexity it exhibits over many length- and time-scales which affects greatly many of their macroscopic properties.[1] A number of recent review articles highlight the general trends in the experimental data as well as in the theoretical models and simulation results.[2−8] Polymer dynamics, which includes vibrational motions, rotations of side groups, the segmental α-process as well as the overall chain dynamics, covers a very broad temporal regime of more than 10 decades from the picosecond (ps) to the second (s) regime;[9] each mode of dynamics may exhibit a different length-scale dependence that needs to be investigated. A number of experimental techniques (neutron and light scattering, dielectric relaxation spectroscopy, nuclear magnetic resonance and others) have been utilized for the investigation of the temporal and/or spatial dependence of polymer dynamics.

One of the simplest types of motion is the methyl group, $-CH_3$, rotation, which can be identified at temperatures lower than the polymer glass transition, T_g;[10] at those temperatures the backbone dynamics is completely frozen and only small side groups may move. The methyl group dynamics has been investigated for several polymers, like poly(methyl methacrylate),[11,12] poly(vinyl methyl ether),[13] polyisoprene,[14] poly(isobutylene),[15] poly(methyl phenyl siloxane),[16] etc. All amorphous systems, on the other hand, exhibit the segmental dynamics or α-relaxation process, which is related to the glass transition. Characteristic features of this process are the nonexponentiality of the respective relaxation function and the non-Arrhenius temperature dependence of its relaxation rate when approaching the T_g. The nonexponential character of the α-relaxation is expressed via the Kohlrausch−Williams−Watts, KWW, relaxation function $\Phi(t) = \exp[-(t/\tau)^{\beta}]$, whereas the temperature dependence of its characteristic time, τ, is empirically described by the Vogel−Fulcher−Tammann expression $\tau \propto \exp[A/(T - T_0)]$. A large number of investigations exist on the segmental relaxation of polymer glasses utilizing a variety of experimental techniques and the main results are summarized in a series of review articles.[2−8]

Received: November 21, 2012
Revised: March 6, 2013
Published: March 25, 2013

The static and dynamic behavior of polymers close to interfaces can be very different from that in the bulk, especially when the molecules are confined to dimensions comparable to their sizes. The dynamics of polymers confined in thin films or within porous media has been attracting the interest of the scientific community for more than a decade; the general trends in the data and the outstanding issues have been highlighted in recent reviews.[17,18] The equivalence in the behavior between polymer nanocomposites and thin polymer films has been quantitatively verified for silica/polystyrene nanocomposites,[19] and studies of the effect of confinement on the glass transition temperature and polymer dynamics have been extended to polymer nanocomposites.[16,19−23]

Polymer nanocomposites containing layered silicates have been widely investigated because of a number of promising applications due to the improvement of mechanical, barrier, flammability, blend compatibilizing, optoelectronic, and other properties. Among the three different types of structures[24,25] (the phase separated, the intercalated and the exfoliated), which exist in such systems depending on the interactions between the polymer and the inorganic surfaces,[26] the intercalated one is of most interest for the studies of structure and dynamics in confinement. In such nanocomposites, a 0.8−2.5 nm polymer film resides between parallel inorganic layers in a well-ordered multilayer with a repeat distance of a few nanometers; this allows the investigation of the effects of nanoconfinement on polymer structure, conformation and dynamics by utilizing conventional analytical techniques on macroscopic specimens. A recent study in intercalated PEO/layered silicate nanocomposites revealed that the polymer chains that are either confined within the galleries of the inorganic material or are adsorbed on the outer surfaces are completely amorphous but possess significantly different conformations than those of the polymer in the melt.[27]

There have been numerous investigations of the dynamics in polymer/layered silicate nanocomposites with results illustrating the influence of both the confinement and the polymer−inorganic interactions on the dynamics. Significantly faster dynamics have been observed for weakly interacting polymers intercalated within inorganic silicate layers in polymer/clay nanocomposites.[16,20,28−31] The significantly faster dynamics within the galleries has been attributed to the suppression of cooperativity,[32] which inherently slows down the dynamics as the glass transition is approached by decreasing temperature, or to enhanced monomeric mobility[33] in an "interphase" region with thickness that can increase with supercooling due to the preferential parallel orientation of the chains near the wall. Alternatively, slower dynamics has been observed as well[34−37] attributed to a 2−9 nm glassy interfacial layer formed when strong attractive interactions exist between the polymer and the solid surfaces. Additionally, poly(ethylene oxide), PEO, confined in hydrophilic layered silicates[29] shows orders of magnitude faster dynamics, which extend below the T_g of the bulk polymer and exhibit a weak Arrhenius temperature dependence. PEO in graphite oxide shows complete suppression of the dielectric α-relaxation,[38] whereas a slowing down of segmental relaxation has been observed in PEO/laponite systems.[35] Moreover, the more local motions like the methyl group rotation or the β-relaxation mode seem to be unaffected by the severe confinement.[16,29]

A new class of versatile materials introduced recently, which hold promise for a broad range of applications, are the hyperbranched polymers (HBPs).[39] HBPs are highly branched macromolecules with three-dimensional almost spherical architecture.[40] They exhibit a tree-like structure (although not as perfect as that of dendrimers) with many branch points emanating from a central core and ending to a large number of functional end-groups per molecule.[41] Therefore, they possess the essential characteristics of dendrimers (globular shape and high end-group functionality) but, at the same time, they are easier and more economical to produce in larger quantities. HBPs are already being utilized as key components in several high-added-value applications (e.g., in nanolithography,[42] as dispersion agents,[43] surface modifiers,[44] processing aids,[45,46] etc.) while they appear as promising candidates for cost-effective pharmaceutical formulations (e.g., drug delivery[47]). However, despite their great industrial importance, only few experimental studies have addressed issues related to their detailed characterization and their structure−property relationships.[48,49] Atomistic molecular dynamics simulations (MD) have been recently performed to probe the behavior of a HBP molecule in the melt, examining certain characteristic static and dynamic properties over different length and time scales.[50] In the case of hyperbranched polymers/layered silicate nanocomposites, very few works have appeared showing that the HBPs with their globular conformations and large number of polar end-groups promote exfoliation for low concentration of clay whereas an intercalated structure is obtained for higher additive concentrations.[51] The nanocomposites show changes in the rheological behavior and an increase in the strength, stiffness and strain at break especially when they exhibit an exfoliated morphology.

In this paper, we investigate the dynamic properties of a hyperbranched polymer, Hybrane S 1200, together with its layered silicate nanocomposites. The dynamics of the systems are experimentally studied by quasi-elastic neutron scattering (QENS). The energy-resolved elastic scattering measurements of the Hybrane show that the elastic intensity relaxes via two steps one below and one above the polymer T_g. Quasi-elastic spectra measured at both temperature regimes probe the characteristics of the sub-T_g and of the segmental relaxation. Deeper insight on the nature of the dynamic processes of the bulk polymer is obtained when the experimental data are quantitatively compared to atomistic molecular dynamics computer simulations performed over a broad temporal range. Further than the investigation of the bulk polymer dynamics, a series of nanohybrids with polymer concentration that covered the whole range from pure polymer to pure clay are synthesized. X-ray diffraction (XRD) measurements show that intercalated structures are formed; nevertheless, achieving this equilibrium structure requires long annealing at elevated temperatures. Differential scanning calorimetry (DSC) results indicate that the glass transition of Hybrane is suppressed when all polymer chains are confined within the inorganic galleries, while the presence of the silicate layers seems to affect the glass transition temperature of the unconfined chains leading to its increase. Moreover, the dynamics of the polymer chains residing within the inorganic galleries is very similar to that of the bulk polymer for temperatures below the bulk T_g; however, the intercalated chains possess completely frozen dynamics at higher temperatures even when all dynamics of the Hybrane in bulk has fully relaxed.

II. EXPERIMENTAL SECTION

Materials. Hybrane S 1200, a hyperbranched polyesteramide[49] with a number-average molecular weight M_n = 1200 g/mol, was kindly

dx.doi.org/10.1021/ma302405q | Macromolecules 2013, 46, 2842−2855

Scheme 1. Chemical structure of Hybrane S 1200

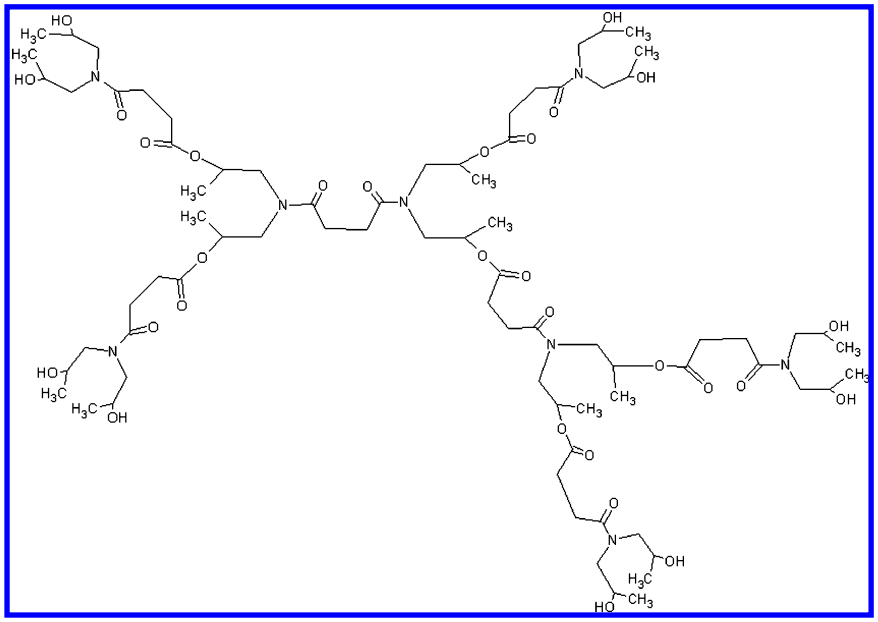

supplied by DSM. The nominal chemical structure of the examined polymer is shown in Scheme 1. The radius of gyration, R_g, of the polymer was calculated utilizing molecular dynamics simulations to be 7.6−8.0 Å with the variation being due to its temperature dependence in the range 350 to 800 K.[50] Hybrane is amorphous with a glass transition temperature, T_g, of 315−320 K (DSM Hybrane Safety Data). The value from our experimental differential scanning calorimetry investigation (to be discussed later) is 315.6K, in agreement with the values in the Safety Data. The specific hyperbranched polymer was chosen because of its hydrophilic character that renders its interactions with the natural hydrophilic clay favorable without the need of surfactant chains, which would complicate the investigation. The inorganic material used in the investigation is sodium montmorillonite, Na^+−MMT (Southern Clay Products, Inc., www.scprod.com). Na^+−MMT exhibits a cation exchange capacity, CEC, of 92.6 mmol/100g and is used after being heated at 120 °C overnight, so that the excess water molecules residing within the hydrophilic galleries are removed. The presence of the Na^+ cations inside the galleries renders them hydrophilic, so that Na^+−MMT can be mixed with hydrophilic polymers such as Hybrane without the need of any surface modifications.

The nanocomposites were prepared using the solution intercalation method. Hybrane was first dissolved in water, which is a good solvent for the polymer whereas it allows swelling of the clay as well. Then, the inorganic component was added, and the suspension was stirred for 1 day. In all cases, special care was taken to ensure that the polymer would be in a dilute solution so that it could be fully dissolved and that the clay would be fully dispersed in the water. The solvent was evaporated in a vacuum oven at room temperature until no further weight reduction could be measured. Finally, all samples were annealed for 24 h at 200 °C under vacuum to erase any metastable structure formed during solvent evaporation and achieve equilibrium. Fourier transform infrared spectroscopy in the attenuated total reflection mode (FTIR-ATR) and thermogravimetric analysis (TGA) measurements are consistent with no degradation occurring during the annealing process under vacuum. Samples with different polymer concentration covering the whole range from pure polymer to pure clay were prepared.

Experimental Techniques. *X-ray Diffraction (XRD).* The structure of the nanocomposites was investigated by X-ray diffraction utilizing a RINT-2000 Rigaku Diffractometer. The X-rays are produced by a 12 kW rotating anode generator with a Cu anode equipped with a secondary pyrolytic graphite monochromator. The wavelength of the Cu Kα radiation used is $\lambda = \lambda_{CuK\alpha} = 1.54$ Å. Measurements were performed for diffraction angles, 2θ, from 1.5° to 30° with step of 0.02°. The layered silicate has a periodic structure, so its XRD pattern is expected to show the characteristic $(00l)$ diffraction peaks, which are related to the spacing of the layers according to Bragg's law, $n\lambda = 2d_{00l} \sin\theta$, where λ is the wavelength of the radiation, d_{00l} the interlayer distance, n the order of diffraction, and 2θ the diffraction angle. In the case of an intercalated system, in which the polymer has entered the inorganic galleries causing an increase of the interlayer distance, this main peak is found shifted toward lower angles. If the structure is exfoliated, however, the ordered structure of the silicate is destroyed and, thus, no peaks are observed in the XRD diffractograms.

Differential Scanning Calorimetry (DSC). The thermal properties of the Hybrane polymer and its nanocomposites were measured with a PL-DSC (Polymer Laboratories) differential scanning calorimeter. The temperature range from −120 to 120 °C was covered with a heating/cooling rate of 10 °C/min. Two heating/cooling cycles were performed in every case and the glass transition temperature, T_g, was obtained from the second cycle to ensure the elimination of any thermal history effects and the removal of any remaining humidity. All the measurements were performed under nitrogen flow to prevent degradation of the samples. Controlled cooling was achieved using liquid nitrogen.

Quasi-Elastic Neutron Scattering (QENS). QENS measures the sum of the coherent, $S_{coh}(q,\omega)$, and the incoherent, $S_{inc}(q,\omega)$, structure factors[52,8] as a function of scattering wavevector, q, and frequency, ω. The measured incoherent and coherent scattering contributions are weighted by the corresponding neutron scattering cross sections. Since the incoherent cross section of hydrogen (σ_{inc}^{H} =79.9 barns) is much higher than both the incoherent and the coherent cross sections, σ_{inc} and σ_{coh}, of all other elements, the scattering is predominately incoherent[53] and is due to the hydrogen atoms in the specimen. The incoherent structure factor, $S_{inc}(q,\omega)$, is the time-Fourier transform of the intermediate incoherent scattering function, $S_{inc}(q,t)$, which is the space−Fourier transform of the Van Hove self-correlation function $G_{self}(r,t)$ that expresses the probability that a considered particle j has experienced a displacement r during a time interval t. In the present paper, we omit the subscript in the notation and limit the discussion concerning the dynamics only to the incoherent contribution.

Quasi-elastic high-resolution neutron backscattering experiments were performed at the IN10 backscattering spectrometer of Institut Laue Langevin (ILL) in Grenoble, France. The energy variation is performed by moving the monochromator and exploring the Doppler effect; the range of energy transfer is set to $-13 < \Delta E = \hbar\omega < 13$ μeV.

dx.doi.org/10.1021/ma302405q | Macromolecules 2013, 46, 2842−2855

The incident wavelength is λ = 6.271 Å, and the scattering vector, q, range was set to $0.5 \leq q \leq 2.0$ Å^{-1} utilizing two small-angle detectors and a two-dimensional curved multidetector.[54] The samples were contained in flat aluminum holders with sample thicknesses $0.2 \leq d \leq 1$ mm. The holders were mounted in a standard ILL cryofurnace. The resulting transmission of the samples is larger than 0.9 and multiple scattering corrections are neglected. The data are corrected for instrumental background by subtraction of an empty sample cell measurement and by taking all shielding contributions into account. The experimental resolution function, $R(q,\omega)$ is obtained by performing measurements at 1.5 K, when the scattering of the samples within the observation window of the instrument is entirely elastic.

The measured dynamic structure factor $S_{exp}(q,\omega)$ is analyzed using a function that includes an elastic and a quasi-elastic contribution to the scattering. The latter is represented by a KWW stretched exponential relaxation function convoluted with the instrumental resolution:

$$S_{exp}(q,\omega) = A_1(q)\left(A_2(q)R(q,\omega) + [1 - A_2(q)]\frac{1}{\pi} FT\{\exp(-(t/\tau)^{\beta})R(q,t)\}\right) \quad (1)$$

$A_2(q)$ is the elastic contribution, τ the relaxation time whereas $R(q,t)$ was obtained analytically by fitting the instrumental resolution function $R(q,\omega)$ with a sum of a Gaussian and a Lorenzian function.[55] $FT\{...\}$ signifies the Fourier transform of the term in $\{...\}$ and $A_1(q)$ is a multiplication factor which accounts for the uncertainty in the exact composition of the silicates and, thus, in their scattering length density.

In addition to the quasi-elastic spectra, the energy-resolved elastically scattered intensity from the samples was measured as a function of temperature in the range $1.5 \leq T \leq 500$ K with a heating rate 0.3 K/min, using an identical setup of monochromator and analyzer. The elastic intensity $I_{el}(q, \omega \approx 0) = \int_{-\infty}^{+\infty} S(q,\omega)R(q,\omega)\, d\omega$ was recorded with the Doppler monochromator at rest corresponding to a resolution of 0.9 μeV. At 1.5K, the samples consist of essentially elastic scatterers; increasing the temperature causes an enhancement of the molecular dynamics, which leads to a decrease of the elastically scattered intensity. The wavevector dependence of the elastically scattered intensity at each temperature can be utilized to extract the mean square displacement, $\langle u^2 \rangle$, assuming a Gaussian behavior in space, according to the equation

$$I_{el(q,\omega\approx 0)} = I_{el(q=0,\omega\approx 0)} \exp(-\langle u^2 \rangle q^2/6) \quad (2)$$

Note that, in many cases, the expression above is utilized with a 3 instead of the 6 in the denominator of the exponential for the calculation of the mean square displacement.

III. MOLECULAR DYNAMICS SIMULATIONS (MD)

Fully atomistic models comprised by 40 Hybrane molecules in the bulk state are generated through the use of the Amorphous Cell algorithm (Materials Studio, Accelrys Inc.). For the description of bonded and nonbonded interactions, energetic parameters according to the AMBER force-field have been utilized;[56] this includes terms corresponding to bond-stretching, angle-bending, torsional rotation, van der Waals, hydrogen-bonding and electrostatic interactions, resulting to a potential energy function of the form

$$E_{total} = \sum_{bonds} K_R(R - R_0)^2 + \sum_{angles} K_\theta(\theta - \theta_0)^2 + \sum_{dihedrals} \frac{V_n}{2}[1 + \cos(n\phi - \delta)] + \sum_{i<j}\left[\frac{A_{ij}}{R_{ij}^{12}} - \frac{B_{ij}}{R_{ij}^{6}}\right] + \sum_{H-bonds}\left[\frac{C_{ij}}{R_{ij}^{12}} - \frac{D_{ij}}{R_{ij}^{10}}\right] + E_{elec} \quad (3)$$

This force-field has been shown to describe satisfactorily hyperbranched compounds of similar chemical composition.[57] Electrostatic interactions are calculated by means of a full Ewald summation. An initial configuration of the melt sample is constructed at an elevated temperature (about 400 K above the expected glass transition temperature) in order to allow a better sampling of the molecular conformations. The system is, then, subjected to cooling MD steps of 50K in the isobaric–isothermal (NPT) ensemble. Ensuing the end of each *NPT* molecular dynamics run, the total energy is minimized through successive steepest descent and conjugate gradient cycles. The cooling process is followed by further equilibration runs in the NPT ensemble, after which the total energy, density and radius of gyration are stabilized. Production runs of 8 ns were generated in the microcanonical (NVE) ensemble employing periodic boundary conditions. The integration time step was 1 fs while the frame-saving frequency was 1 ps. The dimensions of the cubic simulation cell at NVE molecular dynamics runs at the temperatures examined for this work were approximately 47 Å. Validation of the simulation model was performed by comparing static, dynamic and thermodynamic quantities to pertinent experimental results. The density at ambient temperature was found to be 1.15 g/cm^3 which lies within a 2% deviation from the experimental value of 1.18 g/cm^3,[50] while the glass transition temperature as determined from the temperature dependence of the specific volume agrees well with the experimental result.[47] In addition the temperature dependence of the zero shear viscosity as derived from relevant dynamic quantities reproduced the rheologically determined values.[50] Finally, the solubility parameter calculated from the cohesive energy density obtained from the simulations, was in good agreement with pertinent experiments from inverse gas chromatography.[58] For more details concerning the simulation protocol and the validation of the models used, the interested reader is referred to our earlier work.[50]

For a direct comparison to QENS data, the intermediate incoherent dynamic function arising from the scattering of individual atoms was calculated directly in the inverse space, according to

$$S_{inc}(q,t) = \frac{1}{N}\sum_n \langle \exp[i\mathbf{q}\cdot(\mathbf{r}_n(t) - \mathbf{r}_n(0))]\rangle \quad (4)$$

Here, $\mathbf{q}$ represents the scattering vector whose magnitude is equal to q, and $\mathbf{r}_n(t)$ the position vector of the nth scatterer at time t. Since, in incoherent scattering, the observed intensity arises mostly by the motion of individual hydrogen atoms,[53] solely hydrogen atoms have been considered in the calculation of $S(q,t)$ (note that from now on the subscript *inc* is dropped). To shed more light to the origin of the different dynamic processes associated with the diffusive behavior of hydrogens, we have either distinguished between the different sets of hydrogen atoms, i.e., hydrogens belonging to methyl groups, to

hydroxyl groups and to the backbone (see Scheme 1), or have taken all hydrogens into account without making any distinction between them. The so-calculated dynamic spectra are analyzed by determining the distribution of relaxation times (DRT) assuming a continuous superposition of single exponential processes[59]

$$C(t) = \int_{-\infty}^{+\infty} F(\ln(\tau))\mathrm{e}^{-t/\tau}\, \mathrm{d}[\ln \tau] \quad (5)$$

where $F(\ln(\tau))$ is the obtained DRT; the calculated $S(q,t)$ were analyzed utilizing the CONTIN routine of analysis of dynamic light scattering data[59] to obtain the $F(\ln(\tau))$. Characteristic relaxation times corresponding to different motional mechanisms (the latter appearing as different peaks in the distribution) are estimated via the first moment of the calculated distribution function $F(\ln(\tau))$ over the pertinent time range. If the entire time window is taken into account an overall average relaxation time is calculated, instead. For dynamic processes represented by symmetric peaks in the distribution, the time corresponding to the maximum of the examined peak provides a good estimation of the characteristic relaxation time of that process.

IV. RESULTS AND DISCUSSION

Dynamics of Bulk Hybrane. The dynamics of the bulk hyperbranched polymer was investigated using quasi-elastic neutron scattering (QENS). Figure 1a shows the elastic temperature scans for Hybrane at various wavevectors; in such a measurement, only the energy-resolved elastically scattered neutrons are detected and their intensity is measured as a function of temperature. All the curves are shown normalized to the respective data at the lowest temperature where all motions are expected to be frozen. The elastic intensity for the bulk polymer shows two distinct relaxation steps: the first step is a broad decrease at temperatures between ~80 and 220 K. At those temperatures the main chain is still frozen, so the intensity drop should be attributed to local sub-T_g dynamic processes. The most common origin of such sub-T_g motions can be attributed to the more mobile end- and/or side groups, which, in this specific case, are the methyl and the hydroxyl groups attached to the polymer backbone.[16] Additional mechanisms associated with characteristic conformational changes or specific interactions which can give rise to local sub-T_g processes, have also been reported for linear[60] or branched[61] polymers in the past. If this behavior of the elastic intensity is compared to the typical intensity drop associated with the methyl group rotation in the literature,[14,16] it is noticed that the elastic intensity decrease has been usually observed over a narrower temperature range (when measured at spectrometers with similar resolution). This deviation from the anticipated behavior for the $-CH_3$ group rotation indicates that additional dynamic mechanisms could be involved at these length-scales and/or constraints for the motion exist for this particular system. The second step of the elastic intensity for the bulk polymer is observed at temperatures higher than the calorimetric T_g and is caused by the motions of the polymer segments, which become unfrozen above the glass transition temperature. This intensity drop is larger compared to the one attributed to the methyl group rotation, due to the smaller fraction of protons in the methyl groups (48) over their total number (134). Above 420 K, the elastic intensity of the polymer has dropped to values close to zero, indicating that all motions have become too fast for the experimental resolution of the specific instrument. The data in Figure 1, parts b and c, will be discussed in the section describing the dynamics of the Hybrane nanocomposites.

The behavior described above is also reflected in the mean square displacement values, msd, that are extracted from the wavevector dependence of the elastically scattered intensity at each temperature, according to eq 2. Figure 2 shows the msd of the bulk polymer, $\langle u^2 \rangle$, as a function of temperature as well as the respective msd of the layered silicate and the nanocomposite (to be discussed later in the text). The msd of the

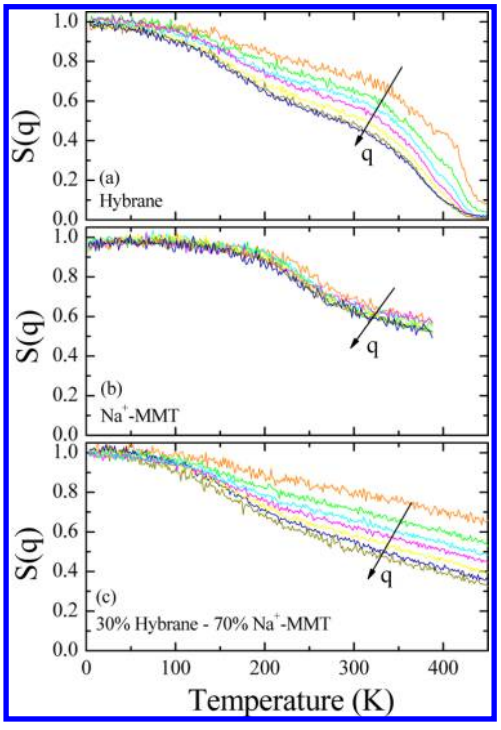

Figure 1. Temperature dependence of the energy-resolved elastically scattered intensity for wavevectors q = 0.5, 0.86, 1.18, 1.45, 1.68, 1.85, and 1.96 Å^{-1} of (a) the Hybrane S 1200, (b) the Na$^+$−MMT, and (c) the 30% Hybrane −70% Na$^+$−MMT nanocomposite. The intensities are shown normalized to those at the lowest temperature for each wavevector.

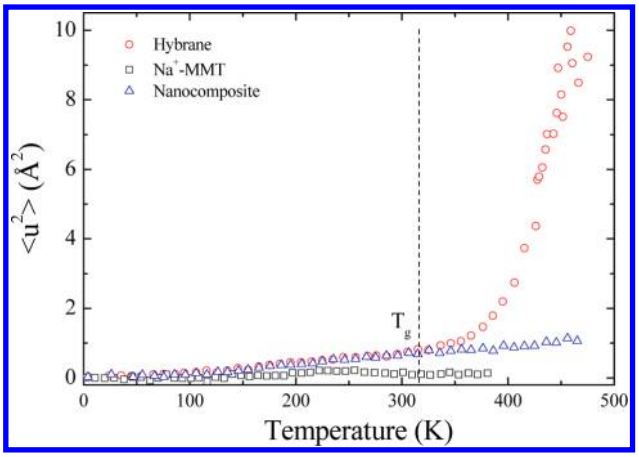

Figure 2. Temperature dependence of the mean square displacement, $\langle u^2 \rangle$, for the Hybrane (○), the Na$^+$−MMT (□) and the 30% Hybrane−70% Na$^+$−MMT nanocomposite (Δ).

polymer is almost insensitive to temperature between T∼2−100 K, it then weakly increases as the sub-T_g dynamic motions set in, it reaches a plateau and then it increases abruptly above the T_g, when the segmental motion becomes active.

QENS measurements have been performed at temperatures covering both the low- and high-temperature regimes, in order to study both the sub-T_g and the segmental motions. Figure 3a shows the temperature dependence of the incoherent dynamic structure factor $S(q,\omega)$ of the polymer for a wavevector q = 1.68 Å^{-1} at temperatures below the glass transition temperature of the polymer. The y-axis is shown at 10% of the maximum intensity at the lowest temperature in order to highlight the spectral wings. The lines for each temperature denote the total fit and the individual elastic and quasi-elastic contributions. In all cases, the stretching parameter β of the KWW was kept constant to the value of β = 0.6; this value gives the best fit simultaneously for all wavevectors and temperatures in good agreement with previous works for the methyl group rotation in polymeric systems.[11,12,14,16] Only a weak temperature effect on the quasi-elastic broadening (expressed as the full-width-at-half-maximum, fwhm, of the curves) can be observed. Figure 3b shows the incoherent structure factor, $S(q,\omega)$, for Hybrane at T = 180 K for different wavevectors with the lines representing the total fits and the elastic and quasi-elastic contributions. The curves are shown at 20% of the maximum intensity at the lowest wavevector. For all wavevectors at this temperature the spectra show a quasi-elastic broadening; nevertheless, this broadening (expressed as the fwhm of the curves) does not show any wavevector dependence. The β parameter that was found to give the best fit for all wavevectors was β = 0.6 as well.[16] Since this temperature as well as the temperatures shown in Figure 3a is below the polymer glass transition temperature, the motion that corresponds to this broadening should be associated with a very local motion, as one would expect for the motion of the end- and/or side groups of the Hybrane molecules, i.e., the methyl and/or the hydroxyl groups.

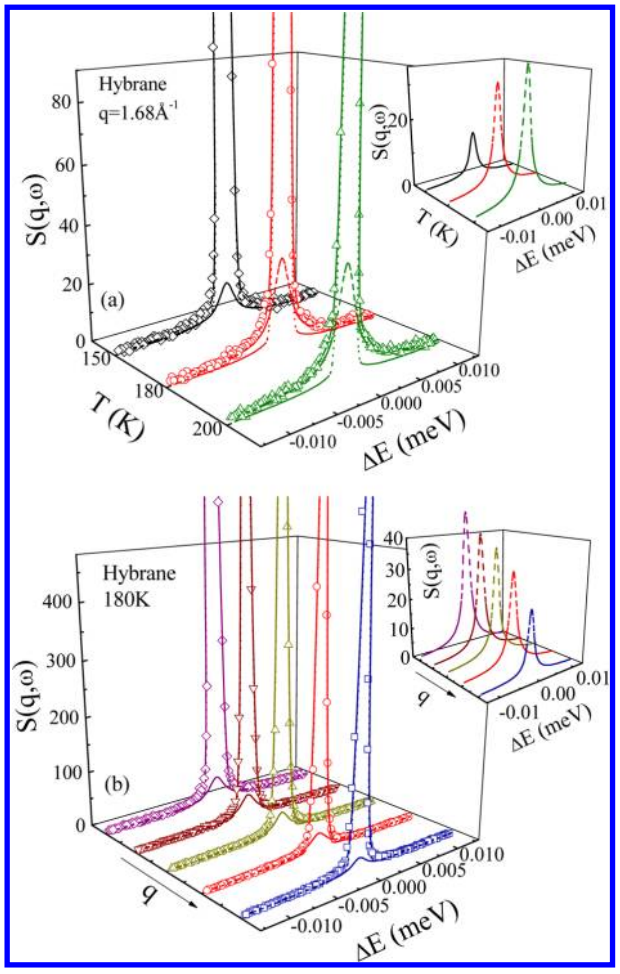

Figure 3. Incoherent structure factor of Hybrane (a) at wavevector q = 1.68 Å^{-1} and at temperatures 150 (◇), 180 (○), and 200 K (Δ), below the polymer glass transition temperature and (b) at T = 180 K for wavevectors q = 0.86 (◇), 1.18 (▽), 1.45 (Δ), 1.68 (○), and 1.96 Å^{-1} (□). The scale of the y-axes corresponds to 10% or 20% of the maximum intensity at the lowest temperature (a) or wavevector (b), respectively. The lines represent the total fit (solid lines) together with the elastic (dotted lines) and the quasi-elastic (dashed lines) contributions to the spectra. The insets shows the respective quasi-elastic part of the spectra for the same temperatures and wavevectors as in the main figures.

The analysis of the experimentally measured incoherent structure factor, $S(q,\omega)$, according to eq 1 leads to the determination of the relaxation times of the respective processes. Figure 4 shows the average relaxation times as a function of the wavevector for Hybrane at all temperatures measured below T_g. The average relaxation time, τ_{ave}, is calculated using the estimated characteristic time of the KWW function used in eq 1, $\tau = \tau_{KWW}$, as $\tau_{ave} = \int_0^\infty \exp[-(t/\tau_{KWW})^\beta]\,dt = (\tau_{KWW}/\beta)\Gamma(1/\beta)$, where β is the stretching exponent and $\Gamma(x)$ the Gamma function with argument x. It is clear that there is no wavevector dependence for any of the measured temperatures and if there is a temperature dependence, it is at best very weak. The absence of any wavevector dependence confirms the presumption that this is a more local relaxation process compared to the length-scale probed in the examined wavevector range.

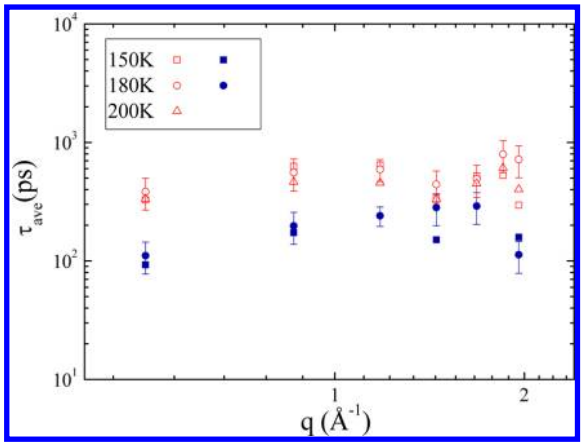

Figure 4. Wavevector dependence of the average relaxation time, τ_{ave}, of Hybrane (open symbols) and of the nanocomposite with 30% Hybrane (solid symbols) for the temperatures indicated, which are lower than the bulk polymer T_g.

Taking as a working hypothesis that this motion arises exclusively from hydrogens belonging to end groups and comparing the observed time scales with those describing the methyl group rotation in other polymers with a less complicated structure, certain deviations are observed. As mentioned earlier, methyl group rotation most often sets in at

dx.doi.org/10.1021/ma302405q | Macromolecules 2013, 46, 2842−2855

lower temperatures (less than 100 K), it is usually observed over a narrower temperature range compared to the present Hybrane case, whereas the temperature dependence of the average relaxation times related to its motion is much stronger. More specifically, if the temperature dependence of the relaxation times in Figure 4 is analyzed with an Arrhenius equation, the extracted activation energy is estimated as E = 0.49 ± 0.25 kJ/mol, which is very much smaller than the values quoted for methyl rotation in other systems.[16,62] This deviation from the anticipated behavior might be related to other types of motion that contribute to the dynamics at these low temperatures and/or to constraints that can modify the mechanism of motion(s), both due to the Hybrane structure.

As it is shown in Scheme 1 depicting the nominal structure, apart from the ten $-CH_3$ groups at the end of the branches, Hybrane has six more $-CH_3$ groups, closer to the molecular core. A possible reason for the observed deviations may be related to the fact that the hydrogens of those methyl groups also contribute to the dynamics, but are less mobile than the ones belonging to the terminal groups. Actually, such a possibility is in accord with computational and experimental results on the dynamics of poly(methyl methacrylate) where the motion of the ester methyl groups was found to be significantly faster than the respective motion of the α-methyls of the molecule.[12,63] Additionally, there are ten $-OH$ end groups, whose hydrogen atoms also contribute to the dynamics at the specific temperature range. Those atoms can act as donors or acceptors in hydrogen bond pairs that are formed between groups of the same molecule (intramolecular) or of neighboring molecules (intermolecular).[50] The existence of hydrogen bonding has been verified experimentally by infrared spectroscopy, via the shifts of the characteristic absorption bands of the carbonyl and hydroxyl groups.[47,64] Moreover, the formation of hydrogen bonds in this system has been studied in detail by molecular simulations in our earlier work.[50] The hydrogen bond survival time correlation functions were calculated and the corresponding time distributions were obtained. Those exhibited two dynamic processes, one associated with the local formation/breaking of the hydrogen-bonded pairs (time range of $O(10^{-2})$ picoseconds, activation energy 5.1 ± 1.1 kJ/mol) and a slower one related to the combined dynamics of the intramolecular hydrogen-bonding network (time range of O(1) to $O(10^3)$ picoseconds depending on the temperature, activation energy of 12.1 ± 0.2 kJ/mol). It was clearly demonstrated that the motion of the hydroxyl groups in Hybrane is drastically affected by the connectivity constraints imposed by the highly branched topology, which results in the formation of a rather firm network of intramolecular hydrogen bonds, quite unlikely to be found in linear polymers. These constraints may influence not only the motion of the hydrogens of the hydroxyl groups but, even more importantly, may hinder the motion of the methyl groups. Thus, it is suggested that it is not simply the motion of the hydroxyl groups that affect the dynamics (their contribution to the intensity would only be 18% of the total) but it is the restrictions that the intramolecular and intermolecular hydrogen bonds (that the hydroxyls form) impose on the motion of the methyl hydrogens as well, which, together with the coupling of the motion of hydrogens belonging to different local groups, could explain the deviations of the present sub-T_g processes from the anticipated behavior for the sub-T_g methyl or hydroxyl group motion. Such restrictions may eventually lead to a change in the mechanism of the usual methyl and/or hydroxyl-group motion, so that a tumbling motion involving local hopping of hydrogens belonging to these spatially restricted groups can be envisaged; such motions result in low apparent activation energies as observed before.[65]

The incoherent structure factor $S(q,\omega)$ for the bulk polymer was measured at temperatures higher than the glass transition temperature as well, i.e., at temperatures above 330 K. Figure 5a shows the temperature dependence of the $S(q,\omega)$, the wings of which show a weak broadening with temperature that is accompanied by a drop of the elastic intensity. Figure 5b shows the wavevector dependence of the incoherent structure factor $S(q,\omega)$ for Hybrane at T = 390 K and the analysis of the experimental data for each q-value, along with the elastic and quasielastic contributions. The stretching parameter β of the KWW was kept constant at β = 0.3 for all curves; this value provided the best fit for all wavevectors whereas it is at the low limit but within the 0.3−0.55 range of β values obtained both experimentally and computationally for the segmental relaxation of different polymers.[66] The incoherent structure factor for the bulk polymer shows a strong wavevector

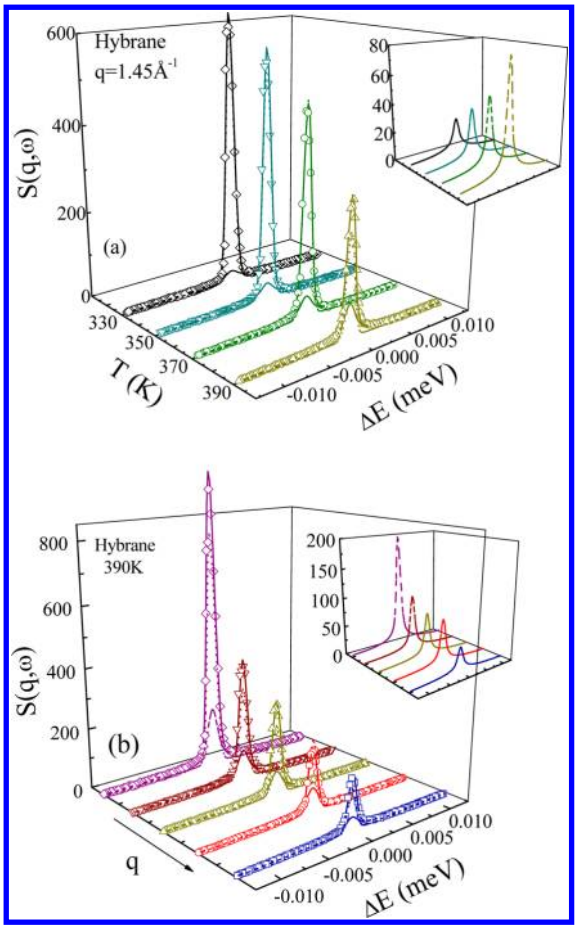

Figure 5. Incoherent structure factor $S(q,\omega)$ of Hybrane (a) at wavevector q = 1.45 Å^{-1} and at temperatures 330 (◇), 350 (▽), 370 (○), and 390 K (△), above the polymer T_g, and (b) at T = 390 K for wavevectors q = 0.86 (◊), 1.18 (▽), 1.45 (△), 1.68 (○), and 1.96 Å^{-1}(□). The lines represent the total fit (solid lines) together with the elastic (dotted lines) and the quasi-elastic (dashed lines) contributions to the spectra. The insets show the respective quasi-elastic part of the spectra for the same temperatures and wavevectors as in the main figures.

dx.doi.org/10.1021/ma302405q | Macromolecules 2013, 46, 2842−2855

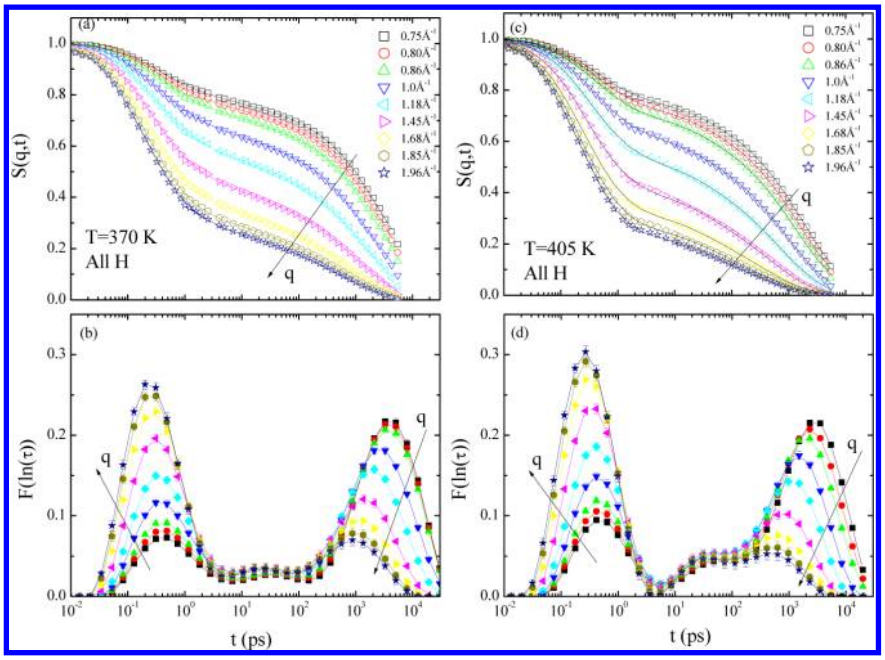

Figure 6. Calculated incoherent structure factor $S(q,t)$ (top row) at temperatures 370 (a) and 405 K (c) for different wavevectors together with the corresponding distributions of relaxation times, $F(\ln(\tau))$ (bottom row), for temperatures 370 (b) and 405 K (d). The lines through the points in the $S(q,t)$ spectra denote the corresponding fits resulted from the DRT analysis (eq 5).

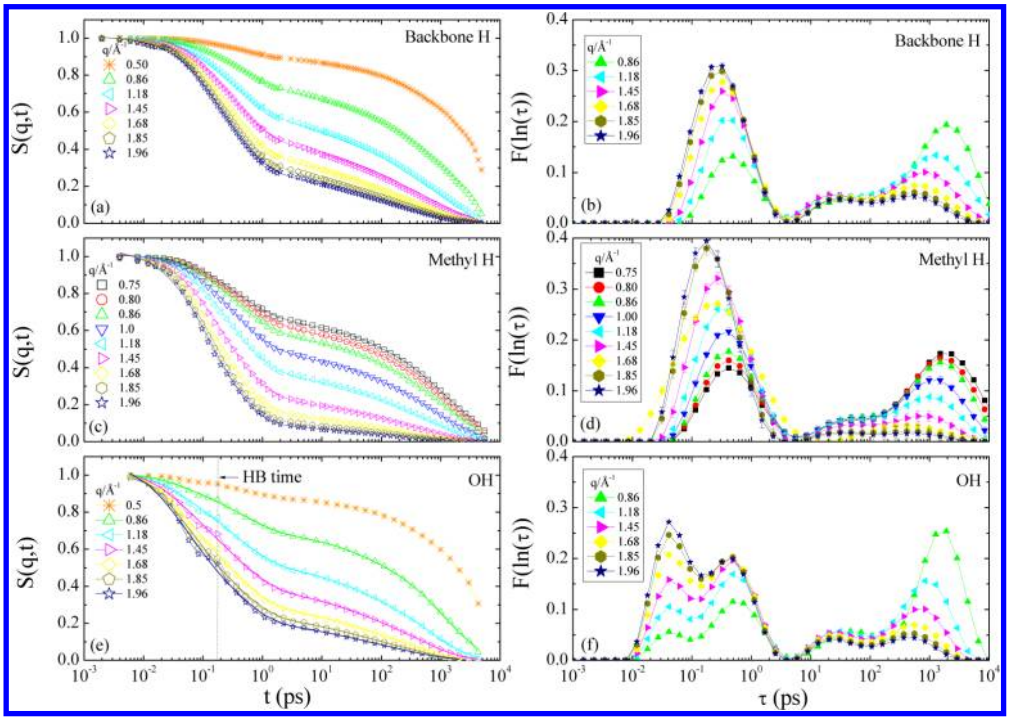

Figure 7. Calculated incoherent structure factor $S(q,t)$ (left column) and corresponding distributions of relaxation times, $F(\ln(\tau))$ (right column), arising from backbone hydrogens (a, b), methyl hydrogens (c, d) and hydroxyl hydrogens (e, f). The lines through the $S(q,t)$ data denote the fits according to the DRT analysis of eq 5. In the case of hydroxyl hydrogens (e), the data are connected with a thinner line as a guide for the eye with the vertical line denoting the time scale of the formation/breaking of the hydrogen bonds (see text).

dependence with the total as well as the elastic intensity decreasing with increasing wavevector (Figure 5b).

In the following, we describe MD simulations, which would assist the interpretation of the QENS data. The MD simulations[50] were carried out at temperatures above T_g so that the $S(q,t)$ spectra will correspond to thermodynamically equilibrated states of the model, which will be sufficiently relaxed within the simulation window so that reliable analysis can be performed. Because of the weak temperature dependence of the broadening of the QENS data over a wide temperature range (both for the local process of Figure 3a and for the relaxation of Figure 5a), it is anticipated that the dynamic information present at lower temperatures will still survive at higher temperatures. To examine dynamic processes

dx.doi.org/10.1021/ma302405q | Macromolecules 2013, 46, 2842−2855

at different time-scales, and at length-scales comparable to those explored experimentally, we have calculated $S(q,t)$ over a broad time-window spanning 6 orders of magnitude (ranging from 10 fs to approximately 10 ns) and for wavevector magnitudes similar to those examined by the neutron scattering experiments described above.

As a first step, to comply with the QENS observables, all hydrogen atoms of every Hybrane molecule were taken into account. The calculated $S(q,t)$ spectra, together with the corresponding distribution of relaxation times, $F(\ln(\tau))$, are presented in Figure 6. One can readily see that the intermediate scattering functions have relaxed almost entirely within the simulation window (to about 80% and 90% for 370 and 405 K, respectively), and the analysis performed (eq 5) provided an excellent fit to the $S(q,t)$ data. Moreover, at both temperatures, the $S(q,t)$ spectra and the corresponding distributions are qualitatively very similar despite the 45 degrees difference in temperature. As the magnitude of the wavevector increases (i.e., the length-scale decreases) the spectra relax faster, as anticipated.

Three peaks characterize the spectra of the DRTs at both temperatures. One at the ps-time scale, which gains amplitude as q increases, a second peak of lower amplitude extending from 10 to 100 ps, which shows no significant dependence of its amplitude on q, and a slower process at the ns-time scale, which loses amplitude upon increasing wavevector (i.e, upon decreasing the examined length-scale). From those spectral characteristics, one can already obtain a first picture regarding the nature of each dynamic process. The features characterizing the faster (leftmost) peak, i.e., the almost wavevector- and temperature-independent time scale at the ps range and its increasing amplitude as q increases, suggest that it should be related to a very local process; it should be at least more local than the length-scale of $2\pi/q$, since, by increasing the magnitude of q, its amplitude continues to increase, implying that the examined length-scale approaches the nominal length-scale of the relevant motional mechanism. Such features are consistent with the very fast tumbling motion of the bond (i.e., C−H or H−O) through which a hydrogen atom is attached to the backbone, to a methyl or to a hydroxyl group. This process characterizes not only the hydrogen motion, but that of more massive atoms, as well.[50] The slower process, described by a temperature-dependent amplitude and characteristic time, which resides at the ns range, bears the characteristics of the polymer α-relaxation. This mechanism reflects the segmental motion of the polymer backbone, which has also been observed in the bond-reorientational motion for the hybrane.[50]

The most intriguing dynamic process, which actually resides within the experimentally accessible window, is that bearing a low-amplitude and almost wavevector- and temperature-independent characteristic time. To further elaborate on the origin of this process, we have examined separately the scattering arising from the different sets of hydrogens present in Hybrane, namely the hydrogens attached to the backbone, the hydrogens of the methyl groups and those of the hydroxyl groups. Figure 7 displays the scattering spectra and the corresponding DRTs for the different kinds of hydrogens, at T = 405 K. Focusing on the DRT spectra (right column of Figure 7), one notices that the slower process associated with the α-relaxation displays similar features for all the different sets of hydrogens as those described earlier in Figure 6 when all hydrogens were taken into account. Distinct differences, however, can be noted in the spectral characteristics of the intermediate process. For the backbone hydrogens (Figure 7b), it appears that the low-amplitude process remains insensitive to variations of the magnitude of the wavevector throughout the examined q-range. In contrast, a rather strong q-dependence of its amplitude is observed when the methyl hydrogens are examined, while an analogous but weaker q-dependence can be seen (at q-values higher than 1.45 to 1.68 Å^{-1}) in the behavior of the hydroxyl hydrogens. Since this intermediate process is observed for all sets of hydrogens, it is possible to associate it with a process that is intimately related to a motion involving the polymer branches, because both the methyl and the hydroxyl groups stem from a polymeric branch and are, thus, directly affected by its motion. A characteristic length-scale for the intermediate process can be inferred approximately by the q-range (i.e., 1.45−1.68 Å^{-1}) at which a q-dependence of its amplitude commences, which yields a length of $l^* = 2\pi/q \sim 4$ Å. The fact that for the backbone hydrogens its amplitude remains less sensitive to q (Figure 7b) implies that backbone hydrogens undergo a somewhat more restricted motion compared to those belonging to the side groups. Finally, in the case of hydroxyl hydrogens, an additional sub-ps process appears in the distribution. This mode can be attributed to the fast hydrogen bond formation/breaking, which was found to be realized at this time scale.[50] This process can be discerned in the scattering function data of Figure 7e at the time scale indicated by the vertical line.

Such very local relaxation mechanisms associated with conformational changes in the polymer backbone, which are active below as well as above the glass transition temperature, have been reported in the literature.[60] Particularly in hyperbranched systems, where strong hydrogen bonding interactions are present, local dynamic processes may arise due to the formed hydrogen-bonding network, which affects the relaxational characteristics of bond and angle reorientation.[61] It is, therefore, reasonable to assume that the strong intramolecular hydrogen-bonding network present in Hybrane plays a significant role in the appearance of the intermediate process.[50] Moreover, since hydrogens attached to side groups are also sensitive to this relaxation mechanism, it can account for the deviations from a typical methyl rotation, as was observed experimentally in the elastically scattered intensity depicted in Figure 4.

The average relaxation times obtained from the analysis of the experimentally measured $S(q, \omega)$ of Hybrane (Figure 5) at temperatures above T_g as well as from the analysis of the corresponding computationally calculated $S(q, t)$ that take into account all the hydrogens of the molecule (Figure 6) are shown in Figure 8, as a function of the wavevector q. The relaxation times obtained from the MD simulation show different wavevector dependencies with the slower segmental relaxation exhibiting the stronger one, as was discussed above. The experimentally measured τ_{ave} values (shown at all three temperatures T = 330 K, T = 370 K, and T = 390 K) lie between the intermediate and the slow processes of the simulation, whereas they exhibit different wavevector dependencies and show an apparent peculiar temperature dependence. At T = 330 K, the experimental relaxation times are q-independent and faster than those at T = 370 K and T = 390 K, with the data at 390 K showing a strong wavevector dependence $\tau_{ave} \sim q^{-2.2\pm0.3}$ that resembles the one anticipated for the segmental dynamics. It is noted that for a Gaussian correlation function, for example for a simple diffusive motion, the relaxation times should follow a $\tau \sim q^{-2/\beta}$ wavevector

dx.doi.org/10.1021/ma302405q | Macromolecules 2013, 46, 2842−2855

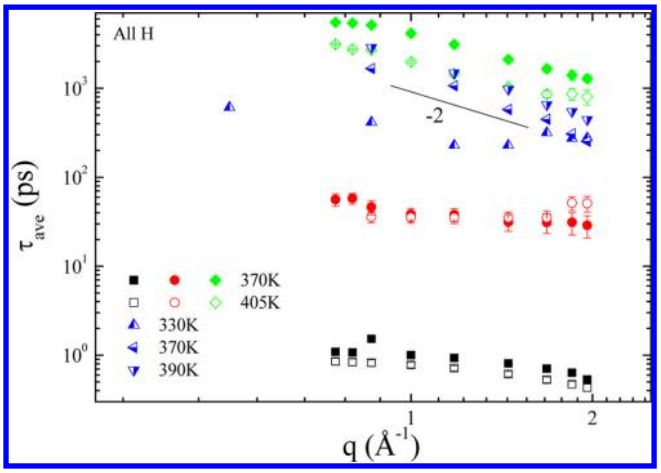

Figure 8. Wavevector dependence of the average relaxation times obtained from the QENS experiments at 330, 370, and 390 K (half-filled symbols) and from the molecular dynamics simulation (T = 370 K solid symbols, T = 405 K open symbols) at temperatures greater than the bulk polymer T_g.

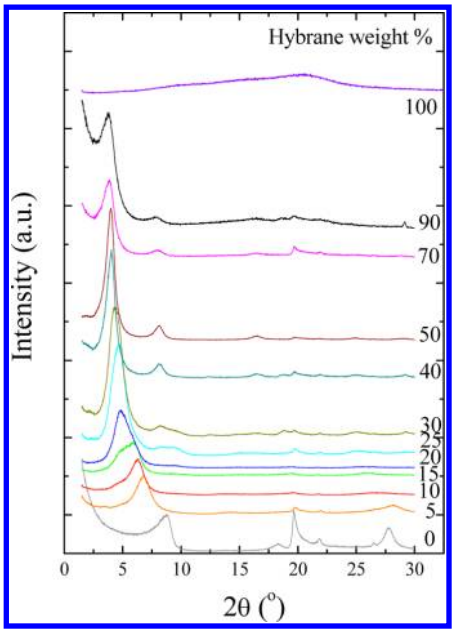

Figure 9. X-ray diffractograms of Na^+−MMT and nanocomposites with varying polymer content prepared by solution mixing and annealed at 200 °C. The wavelength of the Cu Kα radiation $\lambda = \lambda_{CuK\alpha}$ = 1.54 Å has been utilized whereas the curves have been shifted vertically for clarity.

dependence; however, complex heterogeneous dynamics may introduce deviations from this behavior and smaller exponents as well as a crossover from $\tau \sim q^{-2/\beta}$ to $\tau \sim q^{-2}$ have been observed.[16,67] The results concerning the intermediate temperature of 370 K show intermediate behavior as far as the q-dependence is concerned. Moreover, the experimentally measured τ_{ave} at 370 and 390 K are in a good agreement with the results of MD simulation concerning the segmental motion. Thus, it can be concluded that at the lowest temperature the measured spectra are strongly affected by the intermediate process predicted by MD, at intermediate temperatures they are influenced by both processes, and it is only at 390 K that the pure segmental motion is actually observed.

Structure and Dynamics of Hybrane Nanocomposite. A series of Hybrane/Na^+−MMT nanocomposites with polymer compositions that cover the complete composition range have been synthesized utilizing solution intercalation in water followed by slow solvent evaporation and annealing. Figure 9 shows the X-ray diffraction patterns for the inorganic material and the nanocomposites with varying polymer concentration. All samples have been previously annealed for 24h at 200 °C in a vacuum oven to erase any metastable structure formed during solvent evaporation and achieve equilibrium.[31] The high annealing temperature was chosen since attempts for melt intercalation were unsuccessful even at 150 °C whereas lower annealing temperatures did not result in equilibrium.[68] The inorganic material was heated as well to remove any traces of water present in the galleries due to its hydrophilic character. Na^+−MMT shows a main (001) diffraction peak at $2\theta = 8.7° \pm 0.1°$ due to its layered structure, which corresponds to an interlayer distance of d_{001} = 1.05 ± 0.05 nm, in agreement with the value given by the supplier. Hybrane is amorphous and its diffraction pattern exhibits only a weak amorphous halo. The results of the XRD measurements for the nanocomposites indicate that intercalated structures with discrete interlayer distances are formed for all polymer compositions. However, the final structure depends on the polymer content. Upon addition of 5 wt % Hybrane, the silicate main peak shifts to $2\theta = 6.7° \pm 0.1°$, that corresponds to an interlayer distance of d_{001} = 1.30 ± 0.05 nm, which is a result of the polymer chains intercalating within the inorganic galleries. Further increase of the polymer content up to 90 wt % results in the formation of a multilayered polymer structure inside the galleries. The hybrids with 10, 15, 20, and 25 wt % polymer show double peaks corresponding to d_{001} = 1.50 ± 0.05 nm and d_{001} = 1.90 ± 0.05 nm. Further addition of polymer chains forms a third layer inside the galleries increasing the interlayer distance to d_{001} = 2.30 ± 0.05 nm. Note that the second order diffraction peak is clearly visible for high Hybrane concentrations at ∼8°, indicating the good coherence of the structure. An intercalated structure with mono- and bilayers of polymer chains inside the galleries of Na^+−MMT was previously observed in PEO/clay nanocomposites.[29] Moreover, a layer-by-layer intercalation that showed the existence of even four layers of flattened hyperbranched polyester (Boltorn polyols) in montmorillonite was also observed in the past for composites with polymer composition up to 90 wt % whereas partial exfoliation was reported when the polymer was more than 95 wt %.[69] Previous studies on the intercalation behavior of HBPs with different hydroxyl end-groups in polymer/clay nanocomposites have shown a gradual increase of the interlayer distance with the polymer content, leading finally to exfoliation.[51] Depending on the specific interfacial interactions, the confined polymers undergo significant shape changes, they spread out on the surface and adopt flattened conformations.[69,70] Molecular dynamics simulations of dendrimer adsorption on surfaces have predicted that such molecules substantially flatten and spread out onto a surface and generally tend to deform;[70,71] the basic reason for this spreading is the high interaction strength (ionic and/or chemical bonding) between the terminal groups and the substrate surface.

The thermal properties of the polymer nanocomposites were investigated by differential scanning calorimetry (DSC). Figure 10 shows the DSC thermograms of the pure polymer and the intercalated nanocomposites expressed as a heat capacity, for the calculation of which only the polymer mass in considered

dx.doi.org/10.1021/ma302405q | Macromolecules 2013, 46, 2842−2855

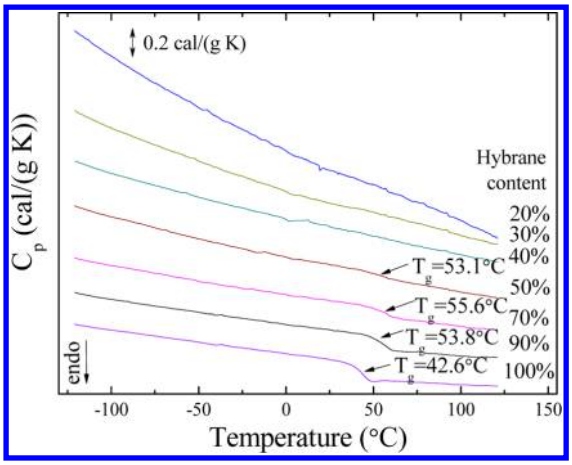

Figure 10. DSC heating curves of Hybrane and of the nanocomposites with varying polymer composition expressed as specific heat, C_p. The curves are shown shifted for clarity.

since the contribution of the inorganic material to the C_p is a constant factor that would not influence the step of the glass transition. The glass transition temperature of the pure polymer is clearly observed at 42.6 °C. However, it is only the nanocomposites with the higher polymer concentrations (>50 wt %) that show a clear glass transition. Hybrids with lower polymer concentrations do not show any step suggesting that the transition is either too weak or too broad to be detected by the technique or that it is suppressed. Similar thermal behavior has been observed in glassy polystyrene/organoclay nanohybrids[72] as well, where there was no trace of the glass transition in the composites in which the polymer chains were intercalated within the inorganic layers. Dielectric spectroscopy measurements in PMPS/organoclay[20] or in PEO/Na^+−MMT[29] hybrids, on the other hand, showed that, when all the chains are intercalated, the segmental motion related to the glass transition becomes very fast and shows an almost Arrhenius temperature dependence. Moreover, the step of the specific heat, ΔC_p, of polymers confined in porous media exhibits a decrease with decreasing pore size; extrapolation to zero ΔC_p, which would indicate a complete suppression of the glass transition, results in a cooperativity length of the order of 1.6−5.0 nm depending on the confined polymer.[73] In the case of Hybrane/Na^+−MMT nanocomposites, the confining length is always the same (smaller than 1 nm) and it is only the polymer concentration that differs between the various samples. The ΔC_p that is calculated taking into account the polymer mass decreases as the polymer content decreases and goes suddenly to zero for polymer concentrations lower than ∼40 wt %.

An explanation that has been proposed for similar hydrophilic systems[31] suggests that for the low polymer content (here less than ∼40 wt %), the majority of chains are intercalated within the inorganic layers and, thus, confinement causes a suppression of the transition. For higher polymer content, there is polymer partially immobilized close to the inorganic surfaces[74] as well as excess polymer away from the surfaces that can undergo a glass transition. Furthermore, the T_g of excess Hybrane (for the composites with high polymer content) is by almost 10 °C higher than that of the pure polymer, indicating that the transition of the nonintercalated chains is affected by the presence of the inorganic surfaces. Particularly for hyperbranched polymers, it has been found that the glass transition depends strongly on the mobility of their terminal groups.[75] Their partial immobilization due to the interaction with the inorganic surface would, therefore, result to a shift of the apparent glass transition to higher temperatures, in line with the experimental findings. This increase of the polymer T_g in the presence of the inorganic galleries has been observed in other hydrophilic polymer/Na^+−MMT nanocomposites as well.[31]

The dynamic behavior of the nanohybrids was investigated utilizing QENS. In order to study the effect of the severe confinement on polymer dynamics the hybrid with 30 wt % polymer was chosen, for which it can be safely assumed that all polymer chains are confined within the galleries of the inorganic material. The energy-resolved elastic scattering for the nanocomposite as a function of temperature is shown in Figure 1c in comparison with the data for the pure polymer (Figure 1a) and those for the pure silicate (Figure 1b). The two steps corresponding to sub-T_g motions and to the segmental relaxation of the polymer have been discussed in the previous section. The elastic intensity of the nanocomposite with 30 wt % Hybrane shows a step-like decrease similar to the respective one of the bulk polymer for low temperatures that once more signifies the insensitivity of the very local end- and/or side-group motion to the present confinement similarly to what has been found for the methyl group rotation of poly(methyl phenyl siloxane)[16] or the dielectrically active β-process of PEO.[29] Nevertheless, for temperatures higher than the Hybrane T_g, the elastic intensity does not drop to zero but shows a continuous decrease that is very similar for all wavevectors. This means that after all sub-T_g motions have relaxed, there is no motion within the experimental window at these temperatures; i.e., the segmental dynamics of the polymer for some reason is suppressed in the proximity of the inorganic surfaces within the galleries. It is noted that the energy-resolved elastic intensity of the pure silicate (Figure 1b) is constant at the lower temperatures and exhibits a step-like decrease around the melting temperature of water. This is attributed to the mobility of water molecules that remain within the galleries, since Na^+−MMT is hydrophilic and contains bound water molecules that are very difficult to escape; those molecules become mobile around 273 K and cause the intensity drop observed in the elastic scattering. As the temperature further increases, this dynamics becomes too fast for the specific frequency resolution and the intensity finally reaches a plateau.

The behavior of the elastic intensities is reflected in the mean square displacement, msd, values that are extracted from their wavevector dependencies, according to eq 2. Figure 2 shows the msd as a function of temperature for the bulk polymer (discussed in the previous section), the silicate and the nanocomposite. It is clear that the msd of the inorganic material is quite small and almost constant throughout the whole temperature range. The corresponding msd of the hybrid shows an initial increase that is very similar to that of the polymer showing the same temperature dependence at the low temperature range ($T < T_g$). Nevertheless, for temperatures above the bulk polymer T_g, the msd does not show any further increase but remains almost constant indicating the absence of any dynamics within the experimental time window of IN10; this indicates that very few, if any, protons participate in the segmental motion of the confined polymer and leads to the conclusion that the majority of the polymer segments must be immobilized onto the inorganic surfaces of the silicate. Such an assumption could justify the absence of any measurable glass

transition for the specific nanohybrid in the DSC measurement of Figure 10.

QENS measurements for the nanohybrid were performed for temperatures both below and above the pure polymer T_g. Figure 11a shows the temperature dependence of the $S(q,\omega)$ of

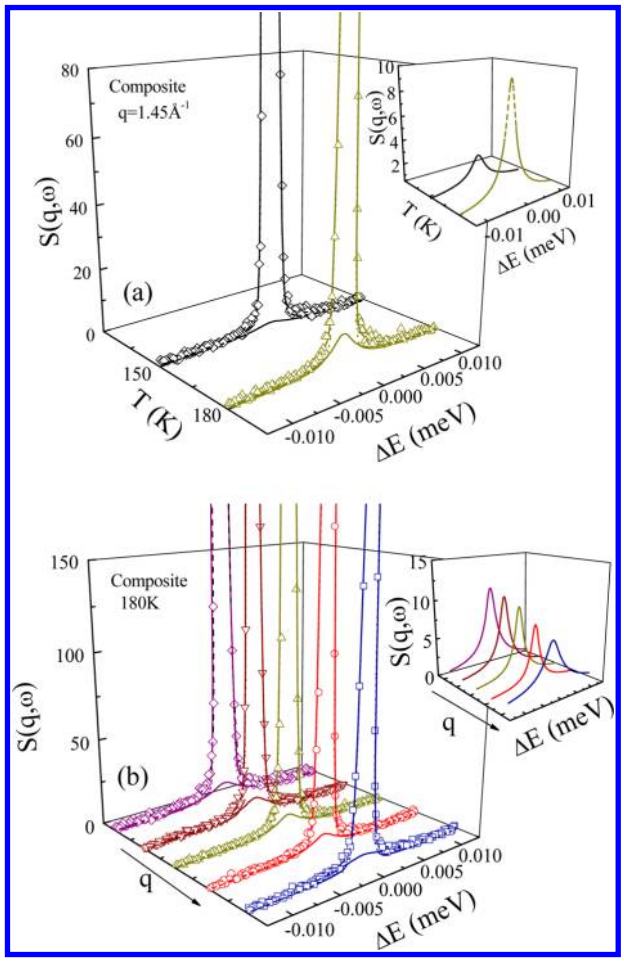

Figure 11. Incoherent structure factor, $S(q,\omega)$, of the nanocomposite with 30% Hybrane (a) at wavevector q = 1.45 Å^{-1} and at temperatures 150 (◊) and 180 K (Δ), below the bulk polymer T_g, and (b) at 180 K for wavevectors q = 0.86 (◊), 1.18 (∇), 1.45 (Δ), 1.68 (○), and 1.96 Å^{-1}(□). The lines represent the total fit (solid lines) together with the elastic (dotted lines) and the quasi-elastic (dashed lines) contributions to the spectra. The scale of the y-axes corresponds to 10% of the maximum intensity at the lowest temperature (a) or wavevector (b). The insets show the respective quasi-elastic part of the spectra for the same temperatures and wavevectors as in the main figures.

the nanocomposite at wavevector q = 1.45 Å^{-1} at temperatures below the polymer glass transition temperature. The weak changes in the broadening of the quasi-elastic wings (dashed lines, inset), expressed as the fwhm of the curves, indicate even weaker temperature dependence than the one of the pure polymer at the corresponding temperatures—especially if all wavevectors are considered. Moreover, the dynamic structure factor of the nanocomposite is almost q-independent; for all wavevectors at 180 K, the spectra (Figure 11b) show quasi-elastic broadening, expressed as the fwhm of the curves, which is almost the same independently of the q value. This behavior is reflected on the relaxation times that can be deduced from the analysis of the data with eq 1 and are shown in Figure 4 together with the results for the pure polymer (the stretching parameter β was kept constant at β = 0.6 as in the bulk polymer). It is clear that there is no wavevector dependence for the average relaxation times, which, for the specific temperature, is found to be somewhat faster for the confined system than for the bulk polymer. The absence of any wavevector dependence in conjunction with the similarity of the relaxation times at temperatures well below the polymer glass transition temperature confirms the assumption that this is a very local relaxation process that is not seriously affected by the confinement of the O(1 nm) between the inorganic layers. The faster dynamics observed in the nanocomposites can be attributed to a reduced number of hydrogen bonds that are formed under confinement, since the molecule does not have the space to retain all possible bulk conformations; this potentially leads to reducing the effects of the constraints on the motion.

Figure 12 shows the experimental $S(q,\omega)$ for the nanocomposite over a broad range of temperatures above the bulk

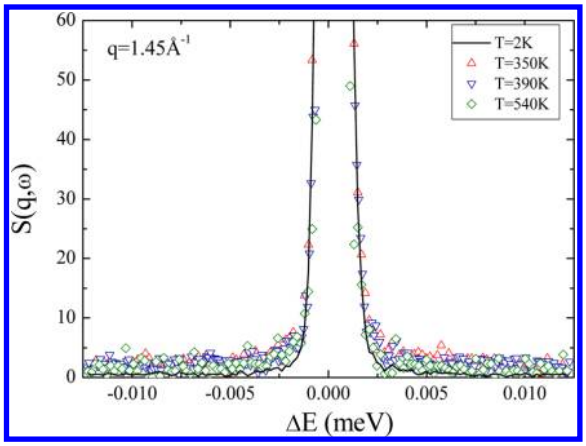

Figure 12. Incoherent structure factor, $S(q,\omega)$, of the nanocomposite with 30% Hybrane for various temperatures above the bulk polymer T_g. The line is the instrumental resolution measured at temperature 2 K. The y-axis is shown at 10% of the intensity of the data for the temperature of 350 K.

polymer glass transition temperature. It is clear that the data do not show any temperature dependence even at the highest temperature measured and that all spectra almost coincide with the instrumental resolution function, indicating frozen dynamics at least for the experimental time range that is accessible by IN10. This result illustrates the effect of both the confinement and the Hybrane/Na$^+$−MMT interactions on the polymer dynamics. This agrees with previous works, where slower dynamics was observed when strong attractive interactions exist between the polymer and the solid surfaces[34−37] as well as with works that obtained a reduction of free volume with the incorporation of layered silicates in polypropylene and polystyrene nanocomposites due to the "solidification" on the clay platelets.[76,77]

V. CONCLUDING REMARKS

The dynamics of a hyperbranched polyesteramide in the bulk and under confinement in polymer/layered silicate nanocomposites has been investigated utilizing quasi-elastic neutron scattering. The energy-resolved elastic intensity for the bulk polymer reveal two relaxation processes one below and one above the polymer glass transition temperature. The quasi-elastic measurements show a sub-T_g process with no wave-

dx.doi.org/10.1021/ma302405q | Macromolecules 2013, 46, 2842−2855

vector dependence and a very weak temperature dependence of its relaxation time. Above T_g, the observed process exhibits peculiar behavior relative to the anticipated segmental mode. Molecular dynamics simulations, performed at high temperatures to understand the dynamic behavior of the bulk polymer, reveal three relaxation processes with different characteristics. The faster is a local motion attributed to the tumbling of the C−H or the O−H bond, the intermediate is related to a motion involving the polymer branches that is influenced by the strong intermolecular hydrogen bonding network existing in hyperbranched polymers whereas the slowest is related to the pure segmental relaxation. The experimentally estimated τ_{ave} values lie between the intermediate and the slow process predicted by MD, being affected by both of these processes and it is only at the highest measured temperature that the segmental behavior is recovered. In the case of the Hybrane/layered silicate nanocomposites, X-ray diffraction measurements show that all hybrids possess intercalated structure (following the necessary thermal annealing), whereas DSC shows no trace of a glass transition when all polymer chains are either intercalated or in the close proximity of the inorganic surfaces. In a nanohybrid, where all chains are strongly confined within the 1.5 nm spacing between the inorganic platelets, both the elastic and quasi-elastic measurements show that, at temperatures below the bulk polymer T_g, the pure and the confined polymer show very similar dynamic behavior whereas, at temperatures above T_g, the confined chains exhibit almost frozen dynamics.

AUTHOR INFORMATION

Present Address

[‖]Nanoscale Materials Science, Swiss Federal Laboratories for Materials Science and Technology (EMPA), Ueberlandstrasse 129, CH-8600, Dübendorf, Switzerland

Notes

The authors declare no competing financial interest.

ACKNOWLEDGMENTS

Part of this research was sponsored by the Greek General Secretariat for Research and Technology (Programme ΣΥΝΕΡΓΑΣΙΑ, 09ΣΥΝ-42-580, and Programme ΠΑΒΕΤ, 05ΠΑΒ96) and by the European Union (Programme CP-IP 246095-2).

REFERENCES

(1) Sakai, V. G.; Arbe, A. *Curr. Opin. Colloid Interface Sci.* **2009**, *14*, 381−390.

(2) Paul, W.; Smith, G. D. *Rep. Prog. Phys.* **2004**, *67*, 1117−1185.

(3) Baschnagel, J.; Varnik, F. *J. Phys: Condens. Matter.* **2005**, *17*, R851−R953.

(4) Lee, H. N.; Paeng, K.; Swallen, S. F.; Ediger, M. D. *Science* **2009**, *323*, 231−234.

(5) Chen, K.; Saltzman, E. J.; Schweizer, K. S. *J. Phys.-Condens. Matt.* **2009**, *21*, 503101.

(6) Roland, C. M. *Macromolecules* **2010**, *43*, 7875−7890.

(7) Freed, K. F. *Acc. Chem. Res.* **2011**, *44*, 194−203.

(8) Colmenero, J.; Arbe, A. *J. Polym. Sci., Part B: Polym. Phys.* **2013**, *51*, 87−113.

(9) Frick, B.; Richter, D. *Science* **1995**, *267*, 1939−1945.

(10) Colmenero, J.; Moreno, A. J.; Alegria, A. *Prog. Polym. Sci.* **2005**, *30*, 1147−1184.

(11) Higgins, J. S.; Allen, G.; Brier, P. N. *Polymer* **1972**, *13*, 157−163;Arrighi, V.; Higgins, J. S.; Burgess, A. N.; Howells, W. S. *Macromolecules* **1995**, 2745−2753.

(12) Chen, C.; Maranas, J. K.; Garcia-Sakai, V. *Macromolecules* **2006**, *39*, 9630−9640.

(13) Chahid, A.; Colmenero, J.; Alegria, A. *Physica A* **1993**, *201*, 101−105. Chahid, A.; Alegria, A.; Colmenero, J. *Macromolecules* **1994**, *27*, 3282−3288.

(14) Frick, B.; Fetters, L. J. *Macromolecules* **1994**, *27*, 974−980;Alvarez, F.; Alegria, A.; Colmenero, J.; Nicholson, T. M.; Davies, G. R. *Macromolecules* **2000**, *33*, 8077−8084;Zorn, R.; Frick, B.; Fetters, L. J. *J. Chem. Phys.* **2002**, *116*, 845−853.

(15) Richter, D.; Arbe, A.; Colmenero, J.; Monkenbusch, M.; Farago, B.; Faust, R. *Macromolecules* **1998**, *31*, 1133−1143. Arbe, A.; Colmenero, J.; Frick, B.; Monkenbusch, M.; Richter, D. *Macromolecules* **1998**, *31*, 4926−4934. Karatasos, K.; Ryckaert, J.-P.; Ricciardi, R.; Laupretre, F. *Macromolecules* **2002**, *35*, 1451−1462.

(16) Chrissopoulou, K.; Anastasiadis, S. H.; Giannelis, E. P.; Frick, B. *J. Chem. Phys.* **2007**, *127*, 144910. Anastasiadis, S. H.; Chrissopoulou, K.; Frick, B. *Mater. Sci. Eng., B* **2008**, *152*, 33−39.

(17) Kumar, S. K.; Krishnamoorti, R. *Ann. Rev. Chem. Biomol. Eng.* **2010**, *1*, 37−58.

(18) Zorn, R.; van Eijck, L.; Koza, M. M.; Frick, B. Special Issue on "Progress in Dynamics in Confinement". *Eur. Phys. J.-Spec. Top.* **2010**, *189*, 1−302. McKenna, G. B. *Eur. Phys. J.-Spec. Top.* **2010**, *189*, 285−302.

(19) Bansal, A.; Yang, H.; Li, C.; Cho, K.; Benicewicz, B. C.; Kumar, S. K.; Schadler, L. S. *Nat. Mater.* **2005**, *4*, 693−698.

(20) Anastasiadis, S. H.; Karatasos, K.; Vlachos, G.; Manias, E.; Giannelis, E. P. *Phys. Rev. Lett.* **2000**, *84*, 915−918.

(21) Ash, B. J.; Siegel, R. W.; Schadler, L. S. *J. Polym. Sci., Part B: Polym. Phys.* **2004**, *42*, 4371−4383.

(22) Kropka, J. M.; Pryamitsyn, V.; Ganesan, V. *Phys. Rev. Lett.* **2008**, *101*, 075702.

(23) Rittigstein, P.; Priestley, R. D.; Broadbelt, L. J.; Torkelson, J. M. *Nat. Mater.* **2007**, *6*, 278−282. Zhang, C.; Guo, Y.; Priestley, R. D. *Macromolecules* **2011**, *44*, 4001−4006.

(24) Pinnavaia, T. J.; and Beall, G. W., *Polymer-Clay Nanocomposites*; John Wiley & Sons: West Sussex, U.K., 2000.

(25) Sinha Ray, S.; Okamoto, M. *Prog. Polym. Sci.* **2003**, *28*, 1539−1641. Tjong, S. C. *Mater. Sci. Eng. Res.* **2006**, *53*, 73−197.

(26) Chrissopoulou, K.; Altintzi, I.; Anastasiadis, S. H.; Giannelis, E. P.; Pitsikalis, M.; Hadjichristidis, N.; Theophilou, N. *Polymer* **2005**, *46*, 12440−12451. Chrissopoulou, K.; Altintzi, I.; Andrianaki, I.; Shemesh, R.; Retsos, H.; Giannelis, E. P.; Anastasiadis, S. H. *J. Polym. Sci., Part B: Polym. Phys.* **2008**, *46*, 2683−2695. Chrissopoulou, K.; Anastasiadis, S. H. *Eur. Polym. J.* **2011**, *47*, 600−613.

(27) Chrissopoulou, K.; Andrikopoulos, K. S.; Fotiadou, S.; Bollas, S.; Karageorgaki, C.; Christofilos, D.; Voyiatzis, G. A.; Anastasiadis, S. H. *Macromolecules* **2011**, *44*, 9710−9722.

(28) Böhning, M.; Goering, H.; Fritz, A.; Brzezinka, K.-W.; Turky, G.; Schönhals, A.; Schartel, B. *Macromolecules* **2005**, *38*, 2764−2774.

(29) Elmahdy, M. M.; Chrissopoulou, K.; Afratis, A.; Floudas, G.; Anastasiadis, S. H. *Macromolecules* **2006**, *39*, 5170−5173. Chrissopoulou, K.; Afratis, A.; Anastasiadis, S. H.; Elmahdy, M. M.; Floudas, G.; Frick, B. *Eur. Phys. J.—Spec. Top.* **2007**, *141*, 267−271.

(30) Mijovic, J.; Lee, H. K.; Kenny, J.; Mays, J. *Macromolecules* **2006**, *39*, 2172−2182.

(31) Fotiadou, S.; Chrissopoulou, K.; Frick, B.; Anastasiadis, S. H. *J. Polym. Sci., Part B: Polym. Phys.* **2010**, *48*, 1658−1667.

(32) Ngai, K. L. *Philos. Mag. B* **2002**, *82*, 291−303.

(33) Mischler, C.; Baschnagel, J.; Binder, K. *Adv. Colloid. Interf. Sci.* **2001**, *94*, 197−227.

(34) Xu, W.; Raychowdhury, S.; Jiang, D. D.; Retsos, H.; Giannelis, E. P. *Small* **2008**, *4*, 662−669.

(35) Lorthioir, C.; Laupretre, F.; Soulestin, J.; Lefebvre, J.-M. *Macromolecules* **2009**, *42*, 218−230.

(36) Hernadez, M.; Carretero-Gonzalez, J.; Verdejo, R.; Ezquerra, T. A.; Lopez-Manchado, M. A. *Macromolecules* **2010**, *43*, 643−651.

(37) Vo, L. T.; Anastasiadis, S. H.; Giannelis, E. P. *Macromolecules* **2011**, *46*, 6162−6171.

(38) Barroso-Bujans, F.; Fernandez-Alfonso, F.; Cerveny, S.; Parker, S. F.; Alegria, A.; Colmenero, J. *Soft Matter* **2011**, *16*, 7173−7176.
(39) Yan, D.; Gao, C.; Frey, H. *Hyperbranched Polymers: Synthesis, Properties and Applications*; Wiley Series on Polymer Engineering and Technology; Wiley: New York, 2011.
(40) Tomalia, D. A. *Mater. Today* **2005**, *8* (3), 35−46.
(41) Hult, A.; Johansson, M.; Malmstrom, E. *Adv. Polym. Sci.* **1999**, *143*, 1−34.
(42) Lebib, A.; Chen, Y.; Cambril, E.; Youinou, P.; Studer, V.; Natali, M.; Pepin, A.; Janssen, H. M.; Sijbesma, R. P. *Microelectron. Eng.* **2002**, *61−2*, 371−377.
(43) Wågbergb, L.; Ondaral, S.; Enarsson, L.-E. *Ind. Eng. Chem. Res.* **2007**, *46*, 2212−2219.
(44) Ondaral, S.; Wågbergb, L.; Enarsson, L.-E. *J. Colloid Interface Sci.* **2006**, *301*, 32−39.
(45) Wang, J. L.; Ye, Z. B.; Subramanian, R.; Kontopoulou, M.; Zhu, S. P. *J. Rheol.* **2008**, *52*, 243.
(46) Anastasiadis, S. H.; Hatzikiriakos, S. G. *J. Rheol.* **1998**, *42*, 795−812.
(47) Suttiruengwong, S.; Rolker, J.; Smirnova, I.; Arlt, W.; Seiler, M.; Luederitz, L.; de Diego, Y. P.; Jansens, P. J. *Pharm. Dev. Technol.* **2006**, *11*, 55−70. Tanis, I.; Karatasos, K.; Assimopoulou, A. N.; Papageorgiou, V. P. *Phys. Chem. Chem. Phys.* **2011**, *13*, 10808−10817.
(48) Gelade, E. T. F.; Goderis, B.; de Koster, C. G.; Meijerink, N.; van Benthem, R.; Fokkens, R.; Nibbering, N. M. M.; Mortensen, K. *Macromolecules* **2001**, *34*, 3552−3558.
(49) Froehling, P. *J. Polym. Sci., Part A: Polym. Chem.* **2004**, *42*, 3110−3115.
(50) Tanis, I.; Tragoudaras, D.; Karatasos, K.; Anastasiadis, S. H. *J. Phys. Chem. B* **2009**, *113*, 5356−5368.
(51) Plummer, C. J. G.; Garamszegi, L.; Leterrier, Y.; Rodlert, M.; Manson, J.-A. E. *Chem. Mater.* **2002**, *14*, 486−488. Rodlert, M.; Plummer, C. J. G.; Garamszegi, L.; Leterrier, Y.; Grünbauer, H. J. M.; Manson, J.-A. E. *Polymer* **2004**, *45*, 949−960.
(52) Bée, M. *Quasielastic Neutron Scattering: Principles and Applications in Solid State Chemistry, Biology and Materials Science*; Adams Hilger: Bristol, U.K., 1988.
(53) Higgins, J. S.; Benoit, H. C. *Polymers and Neutron Scattering*; Oxford University Press: New York, 1994.
(54) Combet, J.; Johnson, M.; Gabriel, A.; Vogl, G.; Petry, W. *Physica B* **2000**, *276−278*, 154−155.
(55) Doxastakis, M.; Chrissopoulou, K.; Aouadi, A.; Frick, B.; Lodge, T. P.; Fytas, G. *J. Chem. Phys.* **2002**, *116*, 4707−4714.
(56) Wang, J.; Cieplak, P.; Kollman, P. A. *J. Comput. Chem.* **2000**, *21*, 1049−1074.
(57) Posocco, P.; Ferrone, M.; Fermeglia, M.; Pricl, S. *Macromolecules* **2007**, *40*, 2257−2266. Lee, H.; Baker, J. R.; Larson, R. G. *J. Phys. Chem. B* **2006**, *110*, 4014−4019.
(58) Dritsas, G. S.; Karatasos, K.; Panayiotou, C. *J. Polym. Sci., Part B: Polym. Phys.* **2008**, *46*, 2166−2172.
(59) Provencher, S. *Comput. Phys. Commun.* **1982**, *27*, 229−242.
(60) Karatasos, K.; Ryckaert, J. P. *Macromolecules* **2001**, *34*, 7232−7235. Arbe, A.; Colmenero, J.; Farago, B.; Monkenbusch, M.; Buchenau, U.; Richter, D. *Chem. Phys.* **2003**, *292*, 295−309.
(61) Turky, G.; Shaaban, S. S.; Schöenhals, A. *J. Appl. Polym. Sci.* **2009**, *113*, 2477−2484. Tanis, I.; Karatasos, K. *Macromolecules* **2009**, *42*, 9581−9591.
(62) Mukhopadhyay, R.; Alegria, A.; Colmenero, J.; Frick, B. *Macromolecules* **1998**, *31*, 3985−3993.
(63) Genix, A.-C.; Arbe, A.; Alvarez, F.; Colmenero, J.; Farago, B.; Wischnewski, A.; Richter, D. *Macromolecules* **2006**, *39*, 6260−6272.
(64) Zagar, E.; Huskic, M.; Grdadolnik, J.; Zigon, M.; Zupancic-Valant, A. *Macromolecules* **2005**, *38*, 3933−3942.
(65) Stride, J. A.; Jayasooriya, U. A.; Nbogo, N.; White, R. P.; Kearley, G. J.; Longeville, S. *Physica B* **2000**, *276−278*, 308−309. Ronemus, A. D.; Vold, R. R.; Vold, R. L. *J. Chem. Soc., Faraday Trans. 1* **1988**, *84*, 3761−3776.
(66) Ahumada, O.; Theodorou, D. N.; Triolo, A.; Arrighi, V.; Karatasos, C.; Ryckaert, J.-P. *Macromolecules* **2002**, *35*, 7110−7124.
(67) Arbe, A.; Colmenero, J.; Alvarez, F.; Monkenbusch, M.; Richter, D.; Farago, B.; Frick, B. *Phys. Rev. Lett.* **2002**, *89*, 245701. Arrighi, V.; Gagliardi, S.; Zhang, C.; Ganazzoli, F.; Higgins, J. S.; Ocone, R.; Telling, M. T. F. *Macromolecules* **2003**, *36*, 8738−8748.
(68) The X-ray diffractograms of the hybrids measured directly after solvent evaporation showed interlayer distances that were increasing with polymer content with the nanocomposite with 90 wt % Hybrane not showing any diffraction peak. Based on previous works on similar systems,[31] solution mixing of clays with bulky molecules may result in nonequilibrium structures; equilibrium can be achieved only after thermal annealing. In the current case, annealing for 48 h at 150 °C resulted only in partial deintercalation of the chains and it was only after the annealing at 200 °C that the equilibrium structure was obtained.
(69) Decker, J. J.; Chvalun, S. N.; Nazarenko, S. *Polymer* **2011**, *52*, 3943−3955.
(70) Tsukruk, V. *Adv. Mater.* **1998**, *10*, 253−257.
(71) Singh, M. S.; Sood, R.; Kaur, G.; Sakai, K.; Yoshimura, T.; Esumi, K. *Colloid Polym. Sci.* **2005**, *284*, 74−79.
(72) Vaia, R. A.; Ishii, H.; Giannelis, E. P. *Chem. Mater.* **1993**, *5*, 1694−1696.
(73) Schönhals, A.; Goering, H.; Schick, C. *J. Non-Cryst. Solids* **2002**, *305*, 140−149. Schönhals, A.; Goering, H.; Schick, C.; Frick, B.; Zorn, R. *J. Non-Cryst. Solids* **2005**, *351*, 2668−2677.
(74) Grady, B. P.; Paul, A.; Peters, J. E.; Ford, W. T. *Macromolecules* **2009**, *42*, 6152−6158.
(75) Karatasos, K. *Macromolecules* **2006**, *39*, 4619−4626. Shumilkina, N. A.; Myakushev, V. D.; Tatarinova, E. A.; Gallyamov, M. O.; Khokhlov, A. R.; Buzin, M. I.; Muzafarov, A. M. *Dokl. Chem.* **2005**, *403*, 155−159.
(76) Jamieson, A. M.; Olson, B. G.; Nazarenko, S. Positron Annihilation Lifetime Studies of Free Volume in Heterogeneous Polymer Systems. In *Polymer Physics: from Suspensions to Nanocomposites and Beyond*, Utracki, L. A., Jamieson, A. M., Eds.; Wiley & Sons Inc.: New York, 2010.
(77) Utracki, L. A.; Simha, R. *Macromolecules* **2004**, *37*, 10123−10133.